Journal of Molecular Liquids 356 (2022) 118983

Contents lists available at ScienceDirect

Journal of Molecular Liquids

journal homepage: www.elsevier.com/locate/molliq

Green synthesized superparamagnetic iron oxide nanoparticles for water treatment with alternative recyclability

Yohannes W. Getahun [a,b], Jorge Gardea-Torresdey [c], Felicia S. Manciu [b], Xiujun Li [c,*], Ahmed A. El-Gendy [b,*]

[a] Environmental Science and Engineering, Material Science & Engineering, University of Texas at El Paso, El Paso, TX 79968, USA
[b] Department of Physics, University of Texas at El Paso, El Paso, TX 79968, USA
[c] Department of Chemistry, University of Texas at El Paso, El Paso, TX 79968, USA

ARTICLE INFO

Article history:
Received 24 January 2022
Revised 9 March 2022
Accepted 20 March 2022
Available online 23 March 2022

ABSTRACT

Widely used water treatment methods are based on chemicals that leave residual unwanted impurities, instigating long-term health impacts. Hence, functionalized **m**agnetic **n**ano**p**articles (MNPs) have been used to fill those gabs and are commonly used for metallic adsorption in contaminated waters. High surface to volume ratio of those MNPs allows for a larger capacity of pollutant adsorption. In this study, functionalized iron oxide MNPs are synthesized by a novel green approach using plant phytochemicals with the capability of absorbing multiple organic pollutants. Herein, we studied synthesis of iron oxide MNPs with crude plant extracts using a simple maceration technique. The reaction was supported further by heat treatments at the supercritical condition of ethanol to complete the reduction process to superparamagnetic iron oxide nanoparticles. Our XRD result shows formation of spherical and cubic goethite (before treatment-Y0PL), magnetite (after treatment -Y0PR) and magnetite (after treatment and functionalization-Y0PRP) with an average crystalline size 277, 29, 45 nm respectively. Phytochemicals increased the size and altered texture of nanoparticles. The magnetic properties were measured for magnetization dependence on external magnetic field to show superparamagnetic behavior with Ms = 44 (Hc = 123 Oe), 36 (Hc = 133 Oe) and 13 (Hc = 44 Oe) emu/g for Y0PR, Y0PRP and Y0PL, respectively. Absorption/reduction efficiency of nanoparticles was studied against MB (10–140 mg/L) and 4-NA (0.5–1 mM). As synthesized green nanoparticles absorbed the model dyes above 80% efficiency under a wide range of conditions in a very short time and 94% under optimum conditions. Moreover, this work introduces successful alternative recyclability in particular for weakly magnetic nanoparticles by growing them on the surface of polyvinyl alcohol solid support. Therefore, the green synthesized superparamagnetic iron oxide nanoparticles prepared in this study are easy to synthesize and cost-effective and enviro-friendly water treatment agents.

1. Introduction

Water treatment is one of the most important technologies extensively explored in the last decades due to various point and non-point sources of pollution that have been increasing parallel to agriculture and industrial developments. This made a clean water crisis in every corner of the world [2]. Contaminated water cannot be used for various purposes before it has passed different levels of purification. Especially, water used for domestic purposes needs to meet quality standards [1]; US EPA. n.d.; [11] and WHO, 2011). Consequently, many treatment technologies have been developed and operating in large scale adhering to regulations on water quality standards. However, the common water treatment processes are full of organic and inorganic residuals from added coagulants, flocculants, disinfectants as well as biproducts resulted from reactions of those chemicals with the organic matter, in addition to pollutants from non-point sources (WHO, 2011). The properties of most of these substances do not allow complete recovery from water, which brings an extra challenge of long-term health impacts. Magnetic nanoparticles (MNPs) have been used in water treatment taking their magnetic property as an advantage for recyclability [16]. Higher surface area and minimal residual after treatment are key advantages in using these particles for water treatment purposes. Additionally, less toxicity of iron oxide magnetic nanoparticles have made them an excellent choice for many biomedical and environmental applications, including water remediation [22,23]. Moreover, the surface chemistry of MNPs can be tuned to optimize recovery as well as improve adsorption affinity to specific metal and non-metal pollutants [16].

* Corresponding authors.
E-mail addresses: xli4@utep.edu (X. Li), aelgendy@utep.edu (A.A. El-Gendy).

https://doi.org/10.1016/j.molliq.2022.118983
0167-7322/

Generally, magnetic iron oxide nanoparticles can be synthesized by physical, chemical, and biological methods [20,21]; Abdeen et al., 2016; Fayez et al., 2020). However, most of the chemical methods use hazardous chemicals during synthesis and functionalization, which adds another treatment step to clean water [5,16,17]. In contrast, biological synthesis methods provide safer particles with simple reaction procedures. For example, bacterial enzymes can synthesize iron oxide MNPs, although the process takes several days to weeks. Many of the particles synthesized this way also suffer from weak magnetic property compared to those synthesized using chemical methods. Besides, after reduction of metal precursors, functionalization must continue in distinct process with newer compounds (Majeed et al., 2020). Some other studies have produced iron oxide nanoparticles from plants. However, many of those studies have used strong alkaline solutions in the synthesis or the surface functionalization to increase the magnetic property of their products, for example, synthesis of F_2O_3 MNPs from orange peel [8], Fe_3O_4 MNPs from *Azadirachta indica* (Samrot et al., 2020). Thus, chemicals used in processing the magnetic nanoparticles become source of their toxicity during application.

In the present study, only plant extracts were used as reducing and coating agents. Plant secondary metabolites are made up of various functional groups known for their biological activity but also capable of reducing nanoparticles [5,24,25]. On the top of their reducing power, those phytochemicals can serve as coating agents, both to stabilize the nanoparticles as well as for multidimensional absorption. Reduction and functionalization were done simultaneously using aqueous extracts of shade dried *Azadirachta indica* leaf. Crude leaf extracts of this plant has diverse metabolites including alkaloids, saponins, flavonoids, tannins and phenolic compounds [27,13]. As a result, it has been used for synthesizing magnetic nanoparticles for water treatment and in various medicinal applications [3,20,27]. Therefore, as-synthesized magnetic iron oxide nanoparticles were used directly to preserve the active ingredients by growing them on a solid material to compensate the loss in magneticity that drastically diminishes their recyclability. Thus, in addition to magnetic manipulation, particles were grown on solid PVA surface to enable alternative recovery. The polyvinyl alcohol (PVA) is chosen as solid support due to its thermal stability up to 354.8 °C and can withstand extreme acidity and basicity conditions [15]. Generally, green one-step synthesis is preferred for health, environmental, and economic reasons. Moreover, multifunctional group compounds on the surface of the nanoparticles improvise absorption of multiple organic pollutants, as well as inorganic ions existed in the polluted water. The present findings motivated us to further study adsorption efficiency to specific heavy metals and efficacy to inhibit microbes of sample nanoparticles, which is already included in our upcoming work.

2. Experimental

2.1. Materials

Chemicals used in this study include iron (III) chloride ($Fe(Cl)_3{\cdot}6H_2O$), iron (II) chloride ($Fe(Cl)_2{\cdot}4H_2O$), methylene blue, sodium hydroxide (NaOH), and hydrochloric acid (HCl), Sodium chloride (NaCl), sodium sulphate (Na_2SO_4), sodium nitrate ($NaNO_3$), sodium bicarbonate ($NaHCO_3$), magnesium sulphate ($MgSO_4{\cdot}7H_2O$), calcium sulphate ($CaSO_4$) and potassium chloride (KCl) were directly used as received from Fischer Scientific LLC. Mili Q water was used as a solvent in all the experiments while the mixture of distilled water and ethanol was employed for washing nanoparticles.

2.2. Extraction

Fresh leaves of Neem (*Azardica indica*) were washed with distilled water and collected after shade drying for ten days. Then, dried leaves were hand crushed and stored at 20 °C. In a 250 ml Erlenmeyer flask, 10 g of power leaf was soaked in 100 ml distilled water for 10 min and then heated with incessant stirring for one hour at 80 °C. Extract solution was double filtered using Whatman filter paper and centrifuged to remove any unfiltered dusts and stored at −10 °C for further use.

2.3. Preparation of magnetic nanoparticles

Solution of metal precursors: 0.1 M of $Fe(Cl)_3{\cdot}6H_2O$ and 0.2 M of $Fe(Cl)_2{\cdot}4H_2O$ (1:1) were prepared in one flask. Plant extracts were added to the flask dropwise with vigorous stirring. The solutions turned black in each addition until completely became black when the whole volume of extracts (1:1) was added. This black suspension of nanoparticles was divided into two portions. The first half (Y0PL) was immediately centrifuged and washed then dried at 60 °C for 6 hr before further analysis. The second half was introduced into pressure reactor and heated at 250 °C and 1000psi for two hours (Y0PR). The reactor vessel was allowed to cool and particles were collected with ethanol and then washed several times in distilled water and then in mixture of distilled water and ethanol. Then the nanoparticles were dried and collected in powder forms for characterization. In the case of plant-based nanoparticles (Y0PL), two solutions that vary in the ratio of plant extracts, 1:1 and 1:2 metal : plant ratios were prepared. However, both samples showed the same performance in absorption and similar spectra in UV and XRD but the former one has higher yield. As a result, only the first solution i.e., 0.1 M of $Fe(Cl)_3{\cdot}6H_2O$ and 0.2 M of $Fe(Cl)_2{\cdot}4H_2O$ and plant extracts (1:1) was used in all experiments in this study.

2.4. Functionalization of nanoparticles

During the synthesis process, plant phytochemicals serve as reducing and functionalizing agents in concerted process. Hence, the synthesized nanoparticles (Y0PL) were produced with their modified surfaces. However, the magnetic moment of these particles was very low. To enhance their magnetic property, the particles were put in the pressure reactor at the abovementioned conditions. At the supercritical condition of ethanol, the reduction of the as-synthesized particles were completed and highly magnetic phase of iron oxide nanoparticles were obtained (Y0PR) but lost their surface modifiers in the process. Thus, subsequent functionalization was necessary to recover plant-based compounds on the surface of the nanoparticles. For this purpose, 50 mg of the nanoparticles were taken and added in to 3 ml solution of extracts and stirred overnight for 12 h. Then, particles were washed first with distilled water then with the mixture of distilled water and ethanol and dried at 60 °C (Y0PRP).

2.5. Preparation of MNPs grown on PVA surface

Using lesser cutter, PVA disks of diameter 7 mm and 2 mm thickness were prepared first. Then, 250 mg of Y0PL was dispersed in Mili Q water in 50 ml centrifuge tube to give 5 mg/L concentration. After that, PVA sponge disks were inserted into solution and stirred overnight in orbital shaker at 150 rpm. The disks were white at the beginning but then turned black same as the solution containing the nanoparticles in the first 10 min indicating growth of the nanoparticles on their surfaces. For the sake of stability, however, the disks were allowed to stir for 15 h. They were then

takeout from the flask and air dried for 14 h after rinsing them with distilled water.

2.6. Preparation of chip

The chip was prepared from 1.5 mm an acrylic glass (Poly (methyl methacrylate), (PMMA)) and designed with inlet, outlet channels and nanoparticles grown on PVA surface in the middle and all connected in channels as shown in **Fig. S1**. After nanoparticles/ PVA is inserted in the middle section, clamped with flat mechanical compressors and placed in the oven for 30 min at 120 °C. The final chip would look like as shown in Fig. 1 below.

2.7. Adsorption assay

Nanoparticles were examined for their absorption efficacy towards methyl blue, a model industrial contaminant and 2-nitroanilline, and an additional organic pollutant that exist in polluted water which also has serious health consequences. The stock solution of methylene blue (MB) was prepared in Milli Q water at 10, 20, 40, 80 and 140 mg/L and that of 4-NA at 0.5 mM and 1 mM concentration. Following this, as synthesized, bare, and functionalized nanoparticles were dispersed in each pollutants concentration to give final concentration of 5 mg/L. Before the absorption experiment, mixture solutions were sonicated for 1 min. This mixture was then put in orbital shaker from 5 to 160 min where sample were taken at 5, 10, 20, 40, 80 and 160 min. Magnetic particles were removed easily from eluates using a magnet whereas non-magnetic nanoparticles were removed by centrifugation at 12800 rpm for 10 min. Absorbance of the final solutions was measured in UV-spectroscopy at 200–800 nm for MB containing solutions and 250 to 550 for 4-NA containing solutions. On the other hand, PVA disks with nanoparticles grown on their surface were assembled into microfluidic chip system. The system comprises inlet, outlet and the disk connected in a linear fashion. An appropriate amount of MB solution(5 ml) was transferred to a syringe and fixed at the plumber. The needle is connected to the inlet by polyethylene tube and the outlet to receiving clean vial with the same tube. At the same concentration of MB used above, absorption performance of sample nanoparticles was studied. Furthermore, time elapse was reduced to a range of 2–12 min. Optimum temperature and pH conditions for the performance of nanoparticles incorporated in PVA sponge was also analyzed in a similar setting. Finally, removal efficiency of nanoparticles was calculated as follows [16]:

$$RemovalEfficiency = (1 - \frac{C_i}{C_e})x100\% \quad (1)$$

where C_i and C_e are initial and equilibrium concentrations of adsorbent.

Similarly, the concentration of pollutants at equilibrium by sample absorbents was calculated by the following formula [7].

$$qe = (\frac{C_e - C_i}{m})xV \quad (2)$$

where C_e is adsorbate concentration at equilibrium(mg/L) and C_i is initial adsorbate concentration in solution, respectively; *m* is mass of the adsorbent in grams per unit volume and V is the volume of the mixture solution in litters.

The nonlinear Langumir model was calculated as

$$qe = \frac{q_m K_L C_f}{1 + K_L C_f} \quad (3)$$

3. Results and discussion

3.1. Structural and morphologic properties

3.1.1. X-ray diffraction (XRD)

XRD measurements were carried out using a PANalytical X'Pert PRO XRD with Cu Kα radiation (λ = 0.1548 nm). As seen in Fig. 2 (a), XRD peaks reveals the crystal structure of Geothite for Y0PL and Magnetite for Y0PR and Y0PRP. The average size was calculated using Scherer formula: D = Kλ/βCos θ as shown in Fig. 2(b) revealing larger size for goethite iron oxide. This size increment is due to concentrated solution of crude extracts possesses as many as compounds for the solvent molecules used during extraction. Thus, the surface of nanoparticles is covered by a group of these compounds resulting in a significant transformation of their sizes [10]. Bare and functionalized nanoparticles have comparable sizes because they are same phase nanoparticle except thin layers of surface compounds from plants during functionalization after they transformed to stable magnetic nanoparticles.

3.1.2. Scanning electronic microscope (SEM)

The morphology of the samples has been investigated using Hitachi S-4800 Field Emission Scanning Electron Microscope (FE-SEM) detector type XFlash 6|60 ex, equipped with EDX from Bruker Nano GmbH Berlin, Germany **as shown in Fig. S1. As synthesized iron oxide nanoparticles display majority of spherical with a few of cubic particles with average size of 160 ± 60 nm (Fig. S2 (a-d)). When these particles were exposed to high pressure and temperature, the size was reduced to 100 ± 20 nm (Fig. S2 (e-l) with larger surface area but higher attractive force to the magnets. In the goethite (Y0PL) sample, surface modification by plant extracts meaningfully affected their complete synthesis to magnetic particles, increased size and interaction. Plant phytochemicals are composed of large number of functional groups that would chelate the metallic nanoparticles eventually building strong shell that lessens the magnetic property and crystallographic presentation of particles blocking the electron beams in the SEM machine, hence blurry images. Simple operation on SEM machine also serves as EDX, which provides information related to elemental composition. Prominent peaks with Fe and O label are for iron and oxygen which are the primary elements in the synthesized samples,**

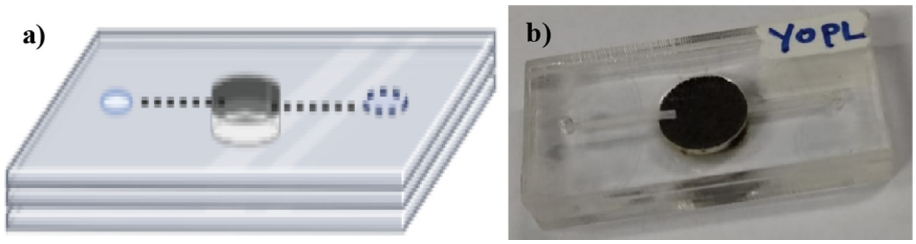

Fig. 1. Continuous single adsorbent Microfluidic chip design: a) 3D-model and b) image of the actual chip.

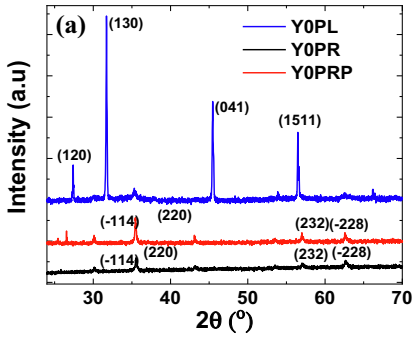

(b)

Material	Crystalline size (Av.) in (nm)	Phase structures
Y0PR	29	Fe3O4- magnetite
Y0PRP	45	Fe3O4- magnetite
Y0PL	277	α-FeOOH- goethite

Fig. 2. XRD pattern of green synthesized nanoparticles(a) crystalline size and phase derived from XRD data (b).

which indicates formation of iron oxide nanoparticles. Other peaks with different elements must have originated from the metal precursors and plant during synthesis or functionalization. Due to their magnetic nature, samples were attached on carbon tape before measurement. Due to that a peak for carbon is shown in the far left in all the EDX graphs (Fig. S2(c, g, k)).

3.1.3. Fourier transformation infrared spectroscopy (FTIR)

The infrared transmission measurements were carried out between 400 and 4000 cm^{-1} with a vacuum based Bruker IFS 66v spectrometer, equipped with a DTGS detector and a KBr beam splitter. The samples for the IR studies were prepared in form of pellets by embedding the Goethite (Y0PL), Magnetite (Y0PR), and Magnetite (Y0PRP) nanoparticles in a transparent polycrystalline CsI matrix. An accumulation of 256 scans was performed for each spectrum. The data were normalized at each frequency to a vacuum throughput spectrum. In Fig. S3, the hydroxyl liberation and the changes in the Fe-O or O-H bonding associated with rearrangement of the oxygen close packing during thermal dihydroxylation from goethite (blue line spectrum) to magnetite (black and red line spectra) are observed. For example, the strong hydroxyl vibrations at 3392 cm^{-1} (stretching), 1629 cm^{-1} (bending), 1398 cm^{-1} (deformation), and 1070 cm^{-1} (deformation) almost disappear in the magnetite spectra of YOPR and YOPRP samples after heat treatment. The Fe-O bands at 687 and 501 cm^{-1} associated with a goethite structural configuration transition to two vibrational modes of FeIII -O at 584 cm-1 and 402 cm-1 (see black spectrum of YOPR) that correspond to a magnetite structure. With nanoparticle functionalization, a downshift in the 584 cm^{-1} vibration to a value of 574 cm^{-1} and disappearance of the 402 cm-1 feature are also observed, demonstrating a further structural transformation.

3.2. Magnetic property

A single step addition of extracts to metal precursors did not result in superparamagnetic nanoparticles that are needed for water treatment application at room temperature. Hence, supporting the reaction by heat treatment at the supercritical condition of liquid was necessary. A portion of these particles was thus heated in pressurized environment. All nanoparticles were attracted to the permanent magnet showing magnetic behavior and their magnetic properties was characterized in vibrating sample magnetometry (VSM) at 300 K and 50 k. During the heat treatment process, the temperature was 250 °C where the magnetic phase structure of Fe3O4 nanoparticles are formed, it is unlikely plant phytochemical will exist in their natural form. Thus, particles were immersed in extract solution and functionalized over 12 h period at room temperature while stirring at 850 rpm. Similarly, these particles were washed and dried to be analyzed in the powder form by the VSM. As shown in Fig. 3, the magnetization dependence on external magnetic field was recorded at 300 and 50 K revealing superparamagnetic-like behavior for all the samples. The saturation magnetization (Ms) and the coercivity (Hc) of both heat-treated nanoparticles (Y0PR) and functionalized after heat treatment (Y0PRP) with 44 and 36 emu/g and 123, 133 Oe respectively have been more than adequate for the intended application which, was possible to easily manipulate the particles in water by a physical magnet as less as 0.5 Tesla. However, magnetic property of functionalized nanoparticles was lower by about 8 emu/g compared to bare counterparts. It is important to note that the first plant-based nanoparticle (Y0PL) has Ms = 13 emu/g and Hc = 44 Oe, which is not feasible for water treatment and hyperthermia or other applications [12].

3.3. Ultraviolet–visible spectroscopy (UV–VIS)

Iron nanoparticles typically display maximum absorbance (λ max) between 300 and 450, which is also shown on the nanoparticles synthesized in the present study (Fig. 4**(a, b)**). The difference between Y0PR and Y0PRP is in the surface property since the latter is modified by plant phytochemicals. Thus, both Y0PR and Y0PRP have similar absorbance maxima. Similarly, Y0PL has identical λ max but narrow peak. Since all samples were measured at the same scan rate, the peak broadening could have been caused by distortion of the electrons while colliding at extreme conditions in the pressure reactor [19]. The bandgap analysis of the samples were determined from Fig. (4b) revealing 3.17, 2.57, and 2. 78 eV for Y0PL, Y0PR, and Y0PRP respectively as shown in Fig. S4.

3.4. Absorption efficiency of nanoparticles towards organic pollutants

3.4.1. Disperison

Dispersion of nanoparticles in aqueous medium enable effective interaction with pollutants in water. Non– functionalized iron oxide nanoparticles are believed to weakly disperse pertinent to metal surface with no binding sites, lacking affinity to water. Good dispersion is also a measure of successful surface modification. In the case of the present magnetic particles, functionalized nanoparticles stood comparatively well dispersed after they were sonicated for 1 h and allowed to stand for another hour. An important finding worth mentioning here is as synthesized nanoparticles (Fig. 5 **III)** were highly dispersed for more than 72 h even after the dispersion. Simultaneous reduction and coating tend to form stable nanoparticles allowing functional groups to grow on the surface during synthesis than attaching on previously stabilized nanoparticles because the attachment is stronger. Nevertheless, their weak magnetic properties would have also significant contribution in preventing their aggregation.

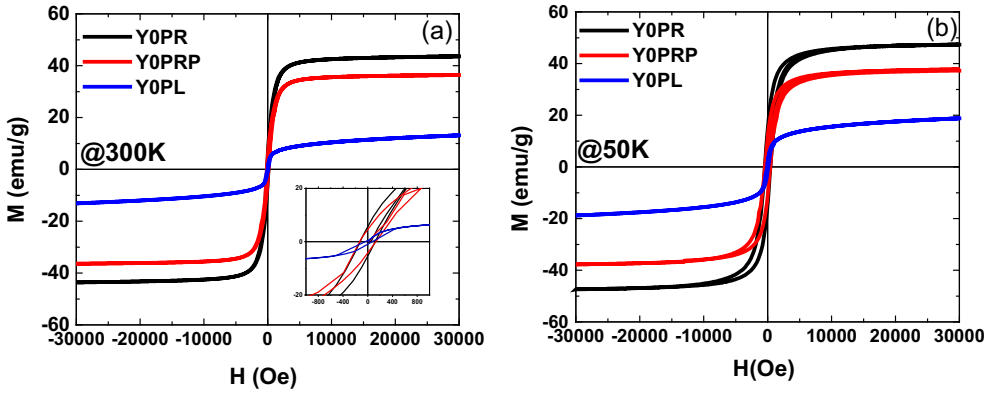

Fig. 3. Hysteresis loop of sample magnetic nanoparticles at room and below room temperature.

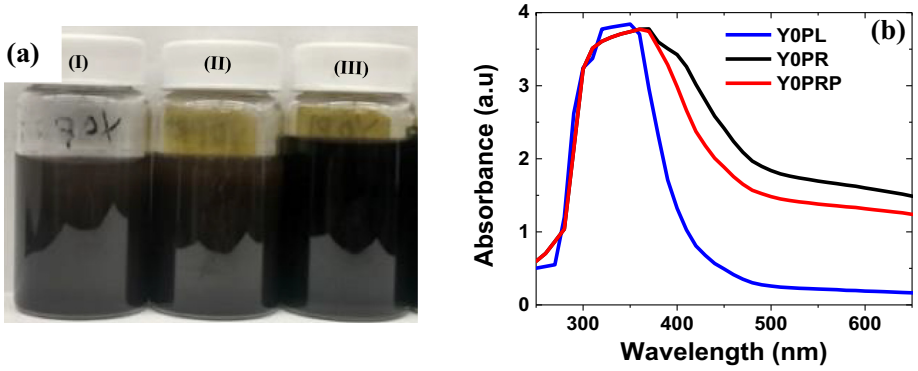

Fig. 4. Green synthesized magnetic nanoparticles: a) Image after synthesis and dispersion (I = Y0PR, II = Y0PRP and III(Y0PL) and b) UV–Vis spectra of the nanoparticles.

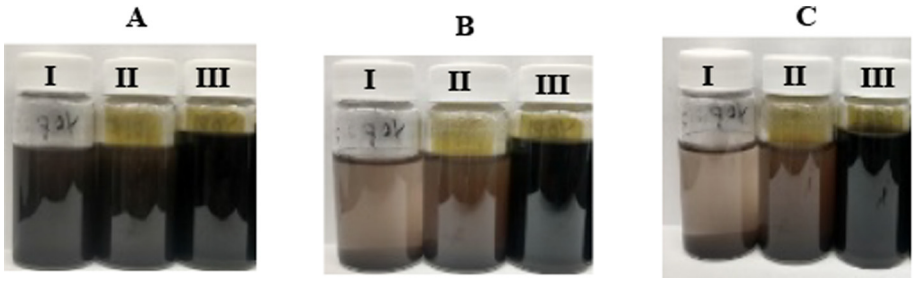

Fig. 5. Dispersion of sample nanoparticles in water at 1 min(A), 30 min (B) and 60 min(C). Where, I = Y0PR, II = Y0PRP and III = Y0PL.

3.4.2. Absorption efficacy of nanoparticles towards methylene blue

The graphs in Fig. 6 represent outputs from absorption experiments of nanoparticles (5 mg/L) added as powders against methylene blue solution at different concentrations (10 to 140 mg/L) and times (5 to 160 min) without addition of catalysts. The absorption spectra for MB at different concentrations can be found in the supplementary material (Fig. S5) Despite its weak magnetic properties, Y0PL showed super performance at all concentrations with above 85% removal efficiency in time less than 20 min. Same amount of adsorbent removed a wide range of concentrations of methylene blue from polluted water. As shown in Fig. 6**(a-f) and Fig. (S6)**, all nanoparticles have high rate of adsorption at their optimum adsorbate concentrations. Both high magnetic samples also showed comparable efficiency for removal of methylene blue at 10 mg/L concentration. However, above this concentration, Y0PL has better efficiency than both bare and functionalized nanoparticles. Y0PR and Y0PRP have comparable small size hence higher surface area, an important factor in absorption mechanism of particles. However, less hydrophilic surfaces prevent them from excellent dispersion in water. This further limits their interaction with pollutants in water at reasonable appropriate time. Even though Y0PRP is functionalized with same solution of extracts, the interaction of the phytochemicals and the nanoparticles should be inadequate due to lack of functional surface on nanoparticles from the pressure reactor.

The adsorption of methylene blue on to sample adsorbent follows Langmuir isotherm. Moreover, calculation of separation factor (R_L) by the formula (4) gives 0.798. R_L value between 0 and 1 signifies favorable adsorption [7].

$$R_L = \frac{1}{1 + K_L C_o} \tag{4}$$

3.4.3. Absorption efficacy of nanoparticles grown on PVA sponge

Effective recyclability of nanoparticles after absorption is the other most important goal of this study. Although, Y0PL was tar-

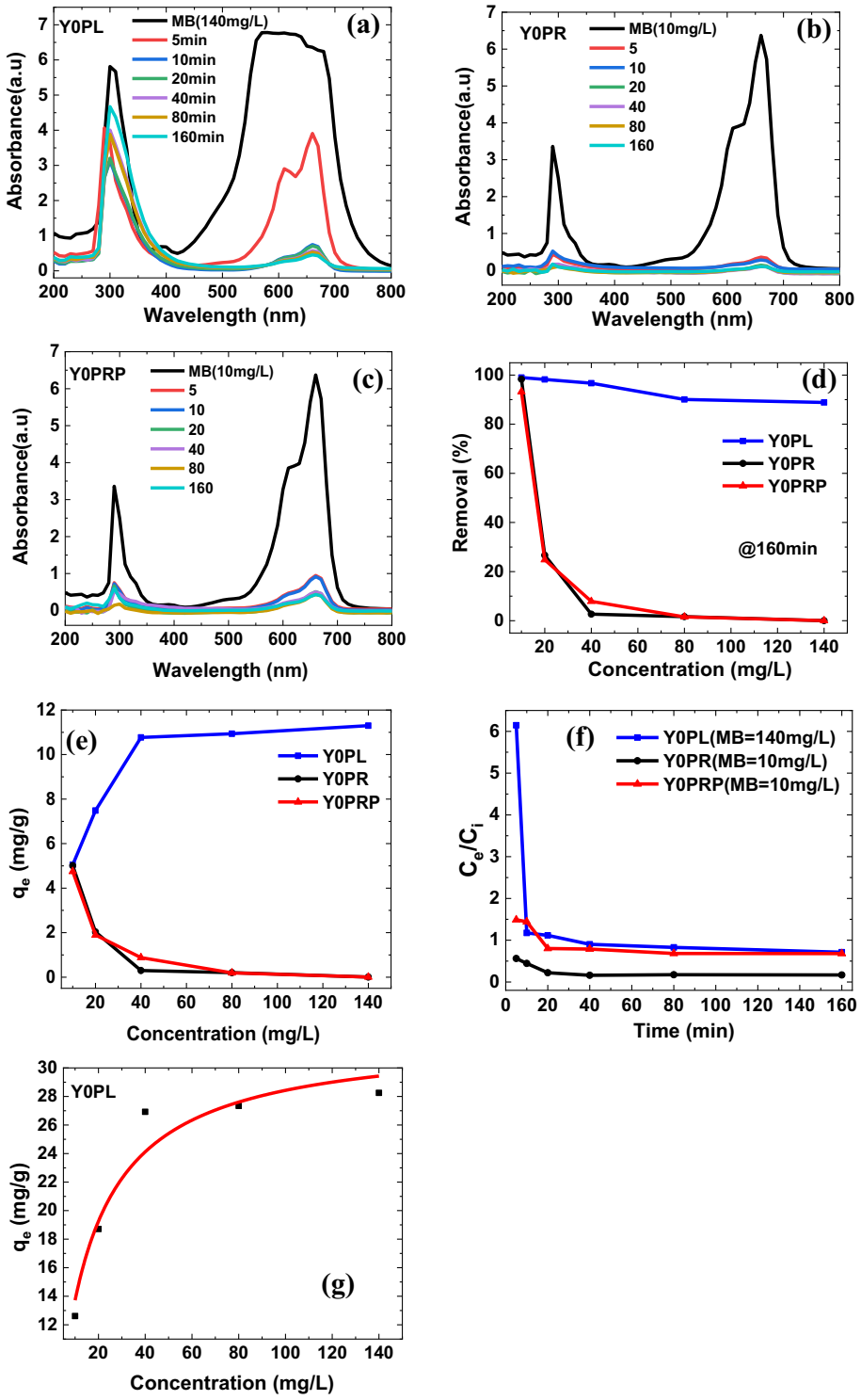

Fig. 6. Absorption efficiency of magnetic nanoparticles towards methylene blue at different time and concentrations (a to f) and non-linear Langmuir isotherm of the highest efficient nanoparticle (g).

geted for this part of the study, all particles grown on PVA disks for comparison purposes between the particles as well as between the methods. Removal efficiency of Y0PL is almost similar; whereas, that of Y0PR and Y0PR was substantially increased to above 80% (Fig. 7(a)). Additionally, contact time has been improved for all nanoparticles to two minutes which is clear in the equilibrium (C_e) to initial concentration (C_i) ratio vs. time curve (Fig. 7(b). As a result, the rate of pollutant removal is also improved. This is because the microfluidic system removes the factor of dispersion out of the equation. First, the particles are localized on PVA disks at the beginning and fixed in adsorbent hole having the size of the disk. Moreover, the system allows specific amount of adsorbate to pass through adsorbents at specific time making many active sites available. When particles are grown on PVA surface during synthesis, excess particles synthesized in the solution may also settle on the top for grown nanoparticles. Some of these do not go

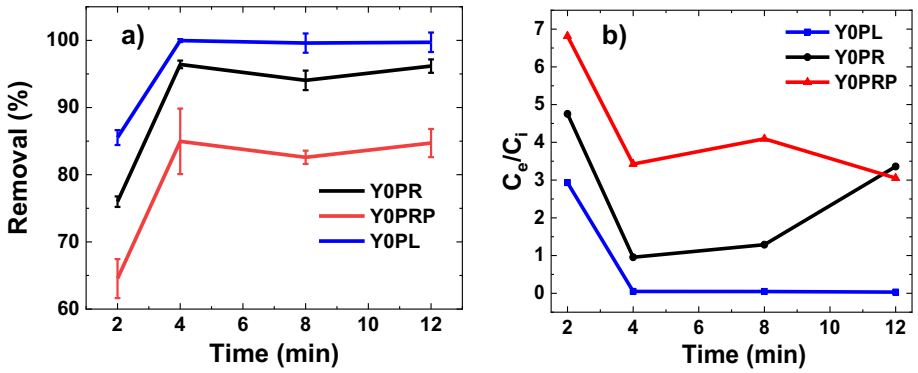

Fig. 7. Percentage of removal of nanoparticles grown on PVA sponge against MB (10 mg/L), pH = 6.6, temperature 21.5 to 23.2. Each experiment was run in triplicates and standard deviations are displayed in error bars.

even washed away with distilled water. Nevertheless, after the disk is dried and placed in the chip system, pollutant solution tends to wash these particles because of pressure. Hence, loosely bound particles along with the die elute in the first two minutes. At optimum conditions, Y0PL has the highest absorption efficacy followed by Y0PR and Y0PRP nanoparticles with comparable performance. The temperature of pollutants during the experiment was from 21.3 to 23.2 °C and pH of methylene blue solution was 6.5.

3.4.4. Effect of pH and temperature on absorption performance of nanoparticles

Effect of temperature and pH on efficiency of nanoparticles was investigated in normal and anticipated extreme conditions in water environment. Absorption results of the particles (Fig. 8) with respect to temperature and pH reveals temperature between 20 and 30 °C and pH between 8 and 12 are conditions for optimum performance for all nanoparticles. Lower temperature (Fig. 8(a)) affects the affinity of pollutants towards the adsorbent due to pollutants agglomeration in condensed water. Similarly, lower pH (Fig. 8(b)) can dissolve nanoparticles as well as alter the surface binding sites of the adsorbent. Since methylene blue is a cationic dye, hydrogen ions must have protonated heteroatoms of surface functional groups creating repulsions between the adsorbent and adsorbate resulting in reduced adsorption [4].

3.4.5. Absorption/Reduction efficacy of nanoparticles towards 2-Nitroaniline

Nanoparticles capable of removing multiple organic pollutants are most preferable in water treatment the fact that contaminated water is rich of many organic and inorganic pollutants. 2-Nitroaniline (4-NA) is another organic pollutant targeted here because of its abundance in the environment and serious health consequences. Removal of 4-NA was studied at 0.5 and 1 mM (Fig. S7) over an interval of time ranging from 5 to 160 min. Findings indicate, Y0PR, Y0PRP and Y0PL absorb/reduce 4-NA 96%, 85% and 26% respectively at 0.5 mM concentration (Fig. 9(a)). Absorption/reduction increased with increase in contact time but decreased with increase in concentration (Fig. 9 (a, b)). Looking at the transformation of the peaks it is important to conclude that the absorption process incorporates reduction of 4-NA to 1, 2-diaminobenzene before treatment, 4-NA has two prominent peaks with λ max at 290 and 410 nm (Fig. 9(c) and after the treatment, the peak at 410 disappears whereas, the peak at 290 nm increases in intensity. This indicates the reduction of nitro into an amine group. The reduction process has non-linear isotherm with R_L = 0.9542 (Fig. 9 (d)).

3.4.6. Effect of ions on removal MB from contaminated water

To investigate the performance of nanoparticles under both organic and inorganic pollutants, multiple ions with concentration that resemble brackish water has added to solution of methylene blue. All other conditions were kept the same with the treatment process done above. No significant change observed for all contact times and concentrations (Fig. 10). On one hand it signifies strong affinity of nanoparticles towards multiple organic pollutants which might have a similar behavior if tested with inorganic ions in the future.

3.4.7. Recyclability

After each treatment, powder nanoparticle was soaked in acetone overnight with vigorous stirring. Then the particles were collected, washed and centrifuged several times with acetone,

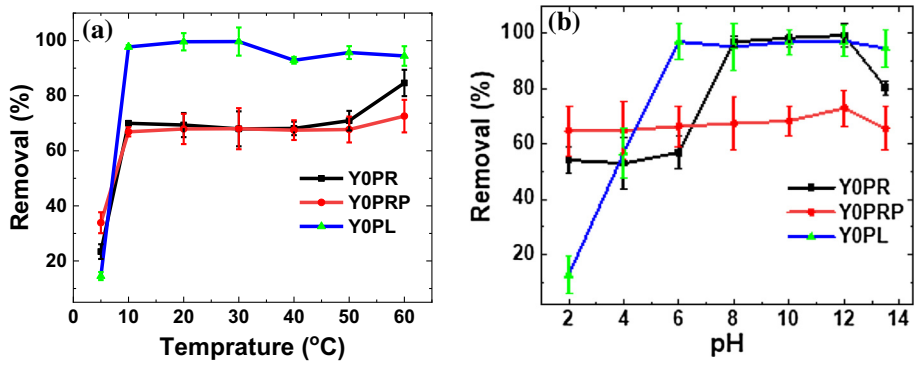

Fig. 8. Optimum conditions for performance of nanoparticles. a) temperature and b) pH. Each experiment was run in triplicates and standard deviations are displayed in error bars.

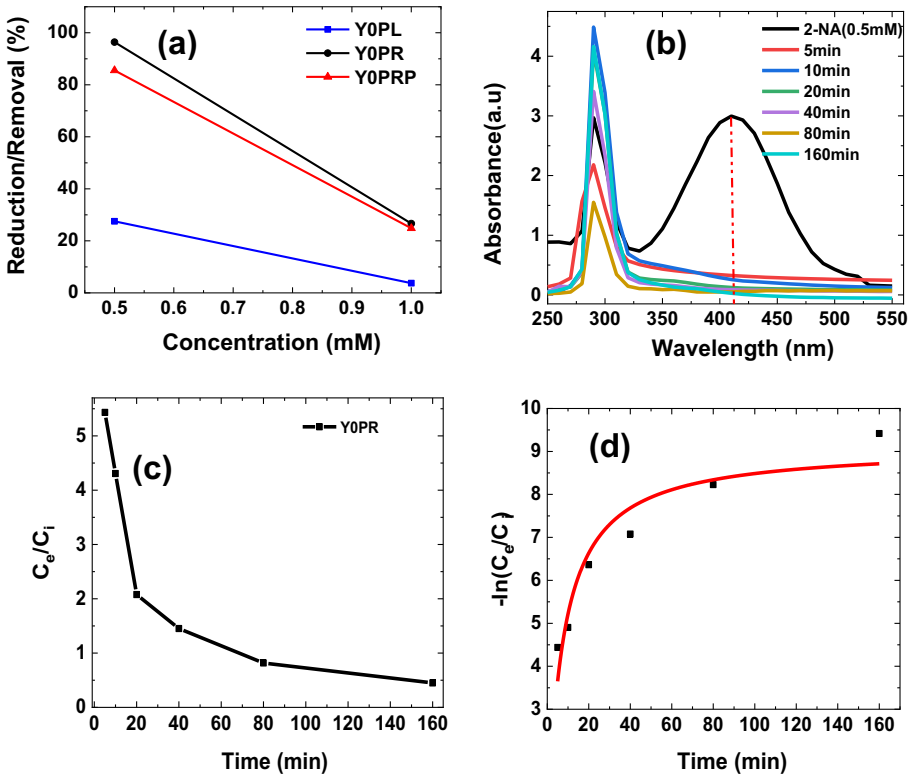

Fig. 9. (a) Absorption/Reduction efficiency of all samples against 4-NA, (b) time dependent degradation of 4-NA by Y0PR, (c) absorbance of degradation of 4-NA by Y0PR at different times, (d) Langmuir isotherm for the degradation of 4-NA by Y0PR.

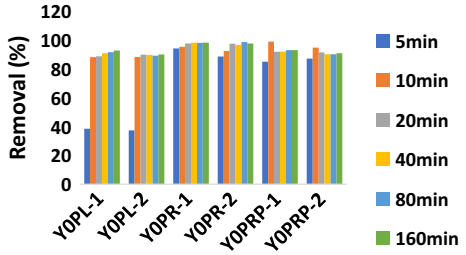

Fig. 10. Effect of ions in the absorption performance of nanoparticles towards methylene blue at different times. Y0PL, Y0PR, Y0PRP (-1) are particles in normal water without ions and Y0PL, Y0PR, Y0PRP (-2) are particles in normal water solution with competitive ions. Each experiment was run in triplicates and standard deviations are displayed in error bars.

distilled water and finally with ethanol and allowed to dry over nigh at 120 °C in an oven. Powder nanoparticle were recovered without losing their efficiency for 5 cycles while particles grown on PVA sponge were washed out after four cycles (Fig. 11 (a, b)). As a result, their absorption capacity declined below 50% after four cycles.

To figure out the efficiency of our nanoparticles in pollutant removal, we have compared our results to the published work of similar magnetic nanoparticles as listed in Table 1. At higher concentration of pollutants, our particles removed efficiently 99.96% of pollutants in a very short time for before and after doped on the solid support polymer for both targeted pollutants. The nanoparticles were more efficient to MB than 4-NA. For the sake of visual evaluation, the photograph images in Fig. S8 displays absorption/reduction efficiency of nanoparticles towards MB and 4-NA. Only

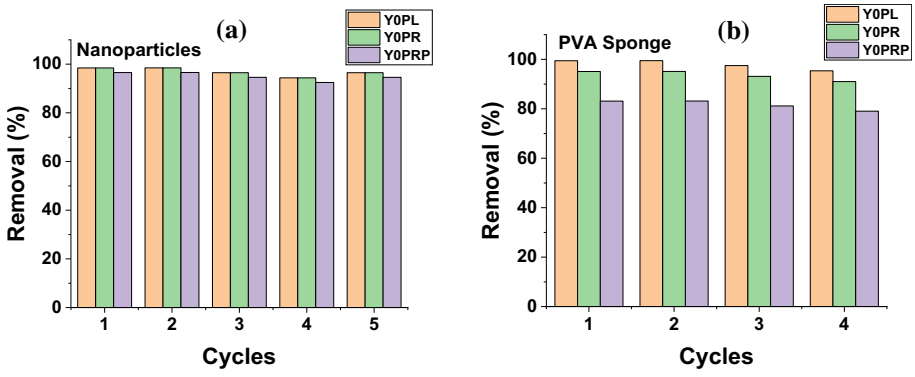

Fig. 11. Recyclability of nanoparticles (a) before and (b) after loading on PVA sponge surface. Each experiment was run in triplicates and standard deviations are displayed in error bars.

Table 1
Pollutant removal comparison of our nanoparticles with recent published work.

Material	Concentration		Optimum conditions		% Removal/ Reduction	Contact time	Ref
	Adsorbent (m)	Absorbate (MB/4-NA)	pH	Temperature (°C)			
γ-Fe_2O_3@Cynometra ramiflorafruit	30 mg	20 mg/L(MB)*	–		94%	120 min	[9]
γ-Fe2O3@ cellulose	0.4 mg/ml	20 mg/L(MB)	5.7	–	~40%	420 min	[28]
Fe_3O_4@graphene oxide	15 mg/L	50 mg/L(MB)	–	30	90%	180 min	[26]
Fe3O4/Fe/Fe3C@PCNF[1]	40 mg + H2O2 catalyst(0.32 M)	100 mg/L	–	85		30 min	[29] Jang et al., 2016 (J. [29]
Fe_3O_4-GO@Polyacrylic acid (PAA)	8 mg/ml	20 mg/L	11	–	100%	1500	
IL/ Fe_3O_4/Ze	0.2 mg/ml + $NaBH_4$(0.5 M)	0.05 M(4-NA)	–		~28%	-	[6] 31w
		0.005 M(MB)	–	–	~47%	–	
NiO	5 mg	0.0145 mM(4-NA) + $NaBH_4$(13.4 mM)	–	40.15	97%	100 min	[18]
Ag@Polymer Microgels	25.2 μg/mL	0.06 mM(4-NA) + NaBH4 (12.64 mM)	9.42	21.1	~90%	22 min	[14]
AgNPs-rGO	1 mM	2 mM(4-NA) + NaBH4 (0.2 mM)	–	–	~87%	20 min	(Y. [30]
AgNPs					~88%	55 min	
Fe_3O_4/α-FeOOH@Azadirachta indica extract	**5 mg/ml**	**140 mg/L(MB)**	**6–12**	**10–30**	**99.96%**	**4 min (Chip)/ 20 min (Powder)**	**This study**
		0.5 mM(4-NA)	**–**	**–**	**83%**	**160 min (Powder)**	

*= photocatalytic degradation.

the highest concentrations at which the nanoparticles show optimum performance are selected for simplicity.

4. Conclusion

In this study, iron oxide nanoparticles are synthesized using a green method that is free of additional chemicals at all processes. Plant phytochemicals acted as reducing and caping agents to form stable magnetite nanoparticles. All nanoparticles showed significant pollutant removal efficiency towards methylene blue and 2-Nitroaniline at a wide range time. Despite their week magnetic property, as synthesized nanoparticles they showed high percentages of removal, even at high concentration of pollutants. Whereas, bare nanoparticles are more efficient in reduction of 4-NA. Particles are efficient at higher pH's of pollutant solution and temperature from 10 to 30 °C, which makes them good candidates in water treatment pertinent to their efficient performance and recyclability at conditions that resemble the actual waste water. Moreover, this work introduces successful alternative recyclability especially, for the weakest magnetic nanoparticles by growing them on the surface polyvinyl alcohol sponge as solid support. In general, green synthesized magnetic nanoparticles in this study are easy to synthesis, cost-effective and enviro-friendly water treatment agents. In our future work, we plan to further investigate absorption efficacy of nanoparticles towards heavy metals as well as study their toxicity to pathogenic microorganisms believed to exist in water.

Declaration of Competing Interest

The authors declare that they have no known competing financial interests or personal relationships that could have appeared to influence the work reported in this paper.

Acknowledgement

A.A.E. acknowledges the startup and rising stars funds by UTEP and UT-system, respectively. A.A.E., J.G.-T and X. L. acknowlage the partial funding by US-National Science Foundation (NSF) (grant number 2009358) and the US-NSF (DMR 1827745, IIP 2122712, and IIP 2052347), NSF ERC (EEC-1449500). Also J.G.-T. acknowledges the Dudley family for the Endowed Research Professorship; the LERR and STARs Retention Award (2018) of the University of Texas System.

Appendix A. Supplementary material

Supplementary data to this article can be found online at https://doi.org/10.1016/j.molliq.2022.118983.

References

[1] V.K. Agrawal, R. Bhalwar, Household Water Purification: Low-Cost Interventions, Med. J. Armed Forces India 65 (3) (2009) 260–263, https://doi.org/10.1016/S0377-1237(09)80019-1.
[2] I. Ali, V.K. Gupta, Advances in water treatment by adsorption technology, Nat. Protoc. 1 (6) (2006) 2661–2667, https://doi.org/10.1038/nprot.2006.370.
[3] M.A. Alzohairy, Therapeutics Role of *Azadirachta indica* (Neem) and Their Active Constituents in Diseases Prevention and Treatment, Evid. Based Complem. Altern. Med. 2016 (2016) 1–11, https://doi.org/10.1155/2016/7382506.
[4] J.O. Amode, J.H. Santos, Z. Md. Alam, A.H. Mirza, C.C. Mei, Adsorption of methylene blue from aqueous solution using untreated and treated (Metroxylon spp.) waste adsorbent: Equilibrium and kinetics studies, Int. J. Ind. Chem. 7 (3) (2016) 333–345, https://doi.org/10.1007/s40090-016-0085-9.
[5] M. Arakha, S. Pal, D. Samantarrai, T.K. Panigrahi, B.C. Mallick, K. Pramanik, B. Mallick, S. Jha, Antimicrobial activity of iron oxide nanoparticle upon modulation of nanoparticle-bacteria interface, Sci. Rep. 5 (1) (2015) 14813, https://doi.org/10.1038/srep14813.
[6] V. Arumugam, K.G. Moodley, A. Dass, R.M. Gengan, D. Ali, S. Alarifi, M. Chandrasekaran, Y. Gao, Ionic liquid covered iron-oxide magnetic

nanoparticles decorated zeolite nanocomposite for excellent catalytic reduction and degradation of environmental toxic organic pollutants and dyes, J. Mol. Liq. 342 (2021) 117492, https://doi.org/10.1016/j.molliq.2021.117492.
[7] N. Ayawei, A.N. Ebelegi, D. Wankasi, Modelling and Interpretation of Adsorption Isotherms, J. Chem. 2017 (2017) 1–11, https://doi.org/10.1155/2017/3039817.
[8] M. Bashir, S. Ali, M.A. Farrukh, Green Synthesis of Fe2O3 Nanoparticles from Orange Peel Extract and a Study of Its Antibacterial Activity, J. Korean Phys. Soc. 76 (9) (2020) 848–854, https://doi.org/10.3938/jkps.76.848.
[9] S. Bishnoi, A. Kumar, R. Selvaraj, Facile synthesis of magnetic iron oxide nanoparticles using inedible Cynometra ramiflora fruit extract waste and their photocatalytic degradation of methylene blue dye, Mater. Res. Bull. 97 (2018) 121–127, https://doi.org/10.1016/j.materresbull.2017.08.040.
[10] A. Borowik, K. Butowska, K. Konkel, R. Banasiuk, N. Derewonko, D. Wyrzykowski, M. Davydenko, V. Cherepanov, V. Styopkin, Y. Prylutskyy, P. Pohl, A. Krolicka, J. Piosik, The Impact of Surface Functionalization on the Biophysical Properties of Silver Nanoparticles, Nanomaterials 9 (7) (2019) 973, https://doi.org/10.3390/nano9070973.
[11] CDC. (2020, November 3). *Drinking water standards and regulations*. Centers for Disease Control and Prevention. Retrieved October 6, 2021, from https://www.cdc.gov/healthywater/drinking/public/regulations.html.
[12] Blazar, D., Getahun, Y., & El Gendy, A. (2021). Magnetic Nanoparticles Hyperthermia, *Magnetic Nanoparticles in Human Health and Medicine: Current Medical Applications and Alternative Therapy of Cancer* (pp. 527–664-512). John Wiley & Sons.
[13] C.P. Devatha, A.K. Thalla, S.Y. Katte, Green synthesis of iron nanoparticles using different leaf extracts for treatment of domestic waste water, J. Cleaner Prod. 139 (2016) 1425–1435, https://doi.org/10.1016/j.jclepro.2016.09.019.
[14] Z.H. Farooqi, K. Naseem, R. Begum, A. Ijaz, Catalytic Reduction of 2-Nitroaniline in Aqueous Medium Using Silver Nanoparticles Functionalized Polymer Microgels, J. Inorg. Organomet. Polym Mater. 25 (6) (2015) 1554–1568, https://doi.org/10.1007/s10904-015-0275-5.
[15] D. Feldman, Poly(Vinyl Alcohol) Recent Contributions to Engineering and Medicine, J. Compos. Sci. 4 (4) (2020) 175, https://doi.org/10.3390/jcs4040175.
[16] J. Guo, R. Wang, W.W. Tjiu, J. Pan, T. Liu, Synthesis of Fe nanoparticles@graphene composites for environmental applications, J. Hazard. Mater. 225–226 (2012) 63–73, https://doi.org/10.1016/j.jhazmat.2012.04.065.
[17] M. Herlekar, S. Barve, R. Kumar, Plant-Mediated Green Synthesis of Iron Nanoparticles, J. Nanoparticles 2014 (2014) 1–9, https://doi.org/10.1155/2014/140614.
[18] Jeon, S., Ko, J. W., & Ko, W. B. (2020). Catalytic Reduction of ortho- and meta-Nitroaniline by Nickel Oxide Nanoparticles. 엘라스토머 및 콤포지트, *55*(3), 191–198. https://doi.org/10.7473/EC.2020.55.3.191
[19] X.C. Jiang, W.M. Chen, C.Y. Chen, S.X. Xiong, A.B. Yu, Role of Temperature in the Growth of Silver Nanoparticles Through a Synergetic Reduction Approach, Nanoscale Res. Lett. (2010), https://doi.org/10.1007/s11671-010-9780-1.
[20] D. Kostyukova, Y.H. Chung, Synthesis of Iron Oxide Nanoparticles Using Isobutanol, J. Nanomater. 2016 (2016) 1–9, https://doi.org/10.1155/2016/4982675.
[21] B.M. Kumfer, K. Shinoda, B. Jeyadevan, I.M. Kennedy, Gas-phase flame synthesis and properties of magnetic iron oxide nanoparticles with reduced oxidation state, J. Aerosol Sci. 41 (3) (2010) 257–265, https://doi.org/10.1016/j.jaerosci.2010.01.003.
[22] B. Mahanty, S. Jesudas, A. Padmaprabha, Toxicity of surface functionalized iron oxide nanoparticles toward pure suspension culture and soil microcosm, Environ. Nanotechnol. Monit. Manage. 12 (2019) 100235, https://doi.org/10.1016/j.enmm.2019.100235.
[23] N. Malhotra, J.-S. Lee, R.A.D. Liman, J.M.S. Ruallo, O.B. Villaflores, T.-R. Ger, C.-D. Hsiao, Potential Toxicity of Iron Oxide Magnetic Nanoparticles: A Review, Molecules 25 (14) (2020) 3159, https://doi.org/10.3390/molecules25143159.
[24] G. Marslin, K. Siram, Q. Maqbool, R. Selvakesavan, D. Kruszka, P. Kachlicki, G. Franklin, Secondary Metabolites in the Green Synthesis of Metallic Nanoparticles, Materials 11 (6) (2018) 940, https://doi.org/10.3390/ma11060940.
[25] K. Mohan Kumar, B.K. Mandal, K. Siva Kumar, P. Sreedhara Reddy, B. Sreedhar, Biobased green method to synthesise palladium and iron nanoparticles using Terminalia chebula aqueous extract, Spectrochim. Acta Part A Mol. Biomol. Spectrosc. 102 (2013) 128–133, https://doi.org/10.1016/j.saa.2012.10.015.
[26] N.H. Othman, N.H. Alias, M.Z. Shahruddin, N.F. Abu Bakar, N.R. Nik Him, W.J. Lau, Adsorption kinetics of methylene blue dyes onto magnetic graphene oxide, J. Environ. Chem. Eng. 6 (2) (2018) 2803–2811, https://doi.org/10.1016/j.jece.2018.04.024.
[27] A.V. Samrot, P. Senthilkumar, S. Rashmitha, P. Veera, C.S. Sahithya, Azadirachta indica influenced biosynthesis of SUPER-PARAMAGNETIC IRON-OXIDE nanoparticles and their applications IN tannery water treatment and X-ray imaging, J. Nanostruct. Chem. 8 (3) (2018) 343–351, https://doi.org/10.1007/s40097-018-0279-0.
[28] R. Xiong, Y. Wang, X. Zhang, C. Lu, Facile synthesis of magnetic nanocomposites of cellulose@ultrasmall iron oxide nanoparticles for water treatment, RSC Adv. 4 (43) (2014) 22632–22641, https://doi.org/10.1039/C4RA01397B.
[29] J. Zhang, M.S. Azam, C. Shi, J. Huang, B. Yan, Q. Liu, H. Zeng, Poly(acrylic acid) functionalized magnetic graphene oxide nanocomposite for removal of methylene blue, RSC Adv. 5 (41) (2015) 32272–32282, https://doi.org/10.1039/C5RA01815C.
[30] Y. Zhang, X. Yuan, Y. Wang, Y. Chen, One-pot photochemical synthesis of graphene composites uniformly deposited with silver nanoparticles and their high catalytic activity towards the reduction of 2-nitroaniline, J. Mater. Chem. 22 (15) (2012) 7245, https://doi.org/10.1039/c2jm16455h.